MEASUREMENTS OF COOLING EFFECTIVENESS ALONG THE TIP OF A TURBINE BLADE

Eric L. Couch

Thesis submitted to the Faculty
of the Virginia Polytechnic Institute and State University
in partial fulfillment of the requirements for the degree of

Master of Science
in
Mechanical Engineering

Dr. K. A Thole, Chair
Dr. C. L. Dancey
Dr. P. King

June 20, 2003
Blacksburg, VA

Keywords: gas turbines, film-cooling, tip gap,
microcircuit, blade heat transfer

MEASUREMENTS OF COOLING EFFECTIVENESS ALONG THE TIP OF A TURBINE BLADE

Eric L. Couch

Abstract

In a gas turbine engine, turbine blades are exposed to temperatures above their melting point. Film-cooling and internal cooling techniques can prolong blade life and allow for higher engine temperatures. This study examines a novel cooling technique called a microcircuit, which combines internal convection and pressure side injection on a turbine blade tip. Holes on the tip called dirt purge holes expel dirt from the blade, so other holes are not clogged. Wind tunnel tests are used to observe how effectively dirt purge and microcircuit designs cool the tip. Tip gap size and blowing ratio are varied for different tip cooling configurations.

Results show that the dirt purge holes provide significant film cooling on the leading edge with a small tip gap. Coolant injected from these holes impacts the shroud and floods the tip gap reducing tip leakage flow.

With the addition of a microcircuit, coolant is delivered to a larger area of the tip. In all cases, cooling levels are higher for a small tip gap than a large tip gap. Increased blowing ratio does not have a dramatic effect on microcircuit film-cooling at the midchord but does improve internal cooling from the microcircuit. While the combined dirt purge holes and microcircuit cool the leading edge and midchord areas, there remains a small portion of the trailing edge that is not cooled. Also, results suggest that blowing from the microcircuit diminishes the tip leakage vortex. Overall, the microcircuit appears to be a feasible method for prolonging blade life.

Acknowledgements

I would not have been able to complete this research without those mentioned in this section. I've thoroughly enjoyed working on this project, so I would like to thank the One who created this beautiful world for us to explore.

My personal life has been enriched through many blessings. My family has loved me unconditionally my whole life and has been very supportive throughout my graduate career. I want to thank Mom and Dad for always being there for me; Cheryl for her steadfastness and strength; Danielle for her brightness in mind and manner; Michael for his intellectual selflessness; Lexi for being a source of joy; and Tibbs for being a dog. I also want to thank Brandie, who is my very best friend. You have all brought happiness to my life.

The many colleagues I've had in the VTExCCL lab all deserve mention here including Andrew, Andy, Chris, Dan, Erin, Evan, Jeff, Joe, Michael, Sachin, Will, and William. I wish all of you success in your future endeavors. An honorable mention must go to Erik and Jesse, my fellow constituents of the "Pratt Team"… (Hoe!). It was my privilege to work with you both.

My advisor Dr. Thole has provided guidance and encouragement to me without fail for a year and a half. I am grateful for everything she has taught me. I also want to thank Professor Alley for his dedication to improving technical writing.

The people at Pratt & Whitney have been extremely helpful. It has been my pleasure to work with them, especially Frank Cunha.

I want to thank the wind tunnel as well. It was always good company though sometimes it seemed like it was full of hot air. But, it was ever true through the good and the bad, the high and the low, the laminar and the turbulent. Thanks also to Sub Station II, for noontime nourishment nearly every day.

Contents

Abstract ii
Acknowledgments iii
Nomenclature vi
List of Tables viii
List of Figures ix

1. Introduction 1
    1.1 Microcircuit Description 5
    1.2 Heat Transfer Analyses of a Turbine Blade with a Microcircuit Design 6
    1.3 Research Objectives 9

2. Review of Relevant Literature 19
    2.1 Effects of Relative Motion Between the Tip and Shroud 19
    2.2 Tip Leakage Flow Models 20
    2.3 Tip Heat Transfer Studies 22
    2.4 Uniqueness of Research 27

3. Experimental Facilities and Instrumentation 43
    3.1 Wind Tunnel Facility 43
    3.2 Experimental Instrumentation and Measurement Techniques 51
    3.3 Testing Procedures and Repeatability 60
    3.4 Uncertainty Analysis 62

4. Results and Analysis 93
    4.1 Engine Scaling of Low Speed Wind Tunnel Measurements 94
    4.2 Experimental Test Matrix for Tip Testing 96
    4.3 Static Pressure Measurements for the Flat Tip Case 97
    4.4 Dirt Purge Case 98
    4.5 Microcircuit Case 104

4.6 Heat Transfer Analysis 111

5. Conclusions 138
5.1 Overview of Results 138
5.2 Recommendations for Future Work 140

References 142
Appendix A: Flexible Wall Adjust Mechanism (FWAM) Design 146
Appendix B: Blade Profile Coordinates 150
Appendix C: Material Properties of Alumina 152
Appendix D: Static Pressure Tap Locations 153
Appendix E: Components for Infrared Camera Window Setup 155
Appendix F: Calculations for Uncertainty Analysis 158
Appendix G: Tip Heat Transfer Coefficient Ratio, h_{gc}, Contours 161

Nomenclature

A = effective area
A_c = internal heat transfer area
A_k = effective conduction area
a, b = lengths of sides of camera viewing area
Bi = Biot number
B_X = axial chord
C = true chord
C_p = static pressure coefficient, $C_p = (P_{s,\,local} - P_{s,\,inlet}) / P_{dyn}$
d = dirt purge hole diameter
d_{tw} = tripwire location
H = tunnel height at profile location
h_c = internal heat transfer coefficient
h_g = external heat transfer coefficient
h_{gc} = heat transfer coefficient ratio
I = momentum flux ratio
k = thermal conductivity
L = distance from camera lens to tip surface
P = blade pitch
$P_{dyn,\,inlet}$ = dynamic pressure at the test section inlet
$P_{s,\,inlet}$ = static pressure at the test section inlet
$P_{s,\,local}$ = local static pressure
Q = heat transfer
q'' = heat flux
Re = Reynolds Number
S = span
s = surface distance along the blade from stagnation
T = temperature
Tu = average turbulence levels
Tu_u = turbulence levels based on streamwise (x) fluctuations
Tu_w = turbulence levels based on cross-stream (z) fluctuations
t = thickness
U_{dil} = velocity of air exiting the dilution holes
U, V, W = velocity components for the blade coordinate system
u, v, w = velocity components for the wind tunnel coordinate system
X, Y, Z = blade coordinate system
x, y, z = wind tunnel coordinate system

Greek

ε = surface emissivity
ϕ = blade angle
ϕ = cooling effectiveness, $\phi = (T_\infty - T_{aw}) / (T_\infty - T_c)$
η = adiabatic effectiveness, $\eta = (T_\infty - T_{aw}) / (T_\infty - T_c)$
μ = absolute viscosity
θ = normalized external wall temperature, $\theta = (T_{aw} - T_{s1}) / (T_{aw} - T_c)$

θ = inlet flow angle (stagger angle)
ρ = density

Subscripts
$\overline{}$ = lateral average value at a given axial location
$\overline{\overline{}}$ = area average value
aw = adiabatic wall conditions
avg = averaged value
c = coolant conditions
max = maximum value
∞ = mainstream conditions
g = gas path conditions
b = background conditions
dil = dilution conditions
s1 = external wall conditions
s2 = internal wall conditions
m = metal conditions
rms = root mean square value
e = engine conditions
t = test conditions

List of Tables

Table 3-1 Blade Parameters 64

Table 3-2 Pressure Transducers 64

Table 3-3 Coolant Flows 64

Table 3-4 Steady State Flow Settings 65

Table 3-5 Uncertainties of Reported Values 66

Table 4-1 Summary of Engine and Tunnel Flows 113

Table 4-2 Experimental Test Matrix 114

Table A-1 FWAM Parts List 146

Table C-1 Material Properties of Alumina 152

Table C-2 Material Properties of Resbond 152

Table D-1 Midspan Pressure Tap Locations 153

Table D-2 Shroud Tap Locations 154

List of Figures

Figure 1-1 Cutaway of a Whittle-type turbo-jet engine (Rolls-Royce, 1992). 11

Figure 1-2 A turbine wheel with unshrouded turbine blades (*IHPTET: Technology Teams in Action*)....11

Figure 1-3 A turbine blade a) after operating in a sand laden environment for 8,200 hours and 4,500 flights, and b) before entering an engine and without film cooling holes. Note the scale is in cm. (Blades courtesy of Pratt & Whitney). 12

Figure 1-4 Layout of turbine blades and stator vanes....12

Figure 1-5 Methods of blade cooling are a) film cooling, b) internal convection, and c) impingement (Mattingly, 1996)....13

Figure 1-6 A modern multi-pass turbine blade cooling scheme (Han et al., 1984). 14

Figure 1-7 Plane wall with fluid movement on both sides. 14

Figure 1-8 Plane wall with film cooling. 15

Figure 1-9 Representation of turbine blade tip and shroud orientation with tip leakage. 15

Figure 1-10 Viewed from the direction of the flow, a simplified section of a turbine wheel. Hot gases leak across the gap between the tip and the shroud....16

Figure 1-11 The microcircuit geometry that was tested in this study: a) an isometric view of the blade with part of the blade removed to show the air passages; b) a top view with the tip surface removed; c) a closer view detailing the dirt purge holes in green and the microcircuit passages in blue. Coolant to the dirt purge and microcircuit was supplied by the plenum shown in red (Hohlfeld, 2003). 17

Figure 1-12 Section view of a microcircuit passage....18

Figure 2.1 Diagram of moving wall apparatus used to simulate relative motion between the shroud and tip (Srinivasan and Goldstein, 2003). 29

Figure 2.2 Separation bubble along the pressure side develops into tip leakage vortex off the suction side trailing edge (Bindon, 1989). 30

Figure 2.3 Tip blowing on the pressure side. The injection slots exit the blade tip at a 45° angle (Prasad, 1999). 30

Figure 2.4 Pressure coefficient contours on the shroud for a flat tip without blowing. The tip vortex is located off the suction side near the blade's leading edge, while the *vena contracta* is on the pressure side of the tip near the trailing edge (Prasad, 1999). 31

Figure 2.5 Heat transfer coefficient distribution in W / m^2 K for a flat blade with tip clearance at 1% of the total blade height (Bunker et al., 2000). 32

Figure 2.6 Layout of a) squealer tip and b) winglet tip (Papa et al., 2003). 32

Figure 2.7 Film cooling hole pattern shown from a) the top and b) a side cross sectional view (Kim and Metzger, 1995). 33

Figure 2.8 Experimental setup with computer visualization on the tip surface (Kim and Metzger, 1995). 34

Figure 2.9 Film cooling effectiveness measurements a) made at four positions downstream of film cooling slots for a blowing ratio of M=0.3 and Re=30x10^3, and b) averaged across the span with a blowing ratio of M=0.5 at three different Reynolds numbers (Kim and Metzger, 1995). 35

Figure 2.10 Spanwise averaged effectiveness for a) Re=15,000 at four blowing ratios, b) Re=30,000 at three blowing ratios, and c) Re=45,000 at three blowing ratios (Kim and Metzger, 1995). 36

Figure 2.11 Heat transfer coefficients were examined for four different tip geometries including a) discrete slots, b) round holes, c) pressure side injection, and d) grooved tips (Kim et al., 1995). 37

Figure 2.12 Typical spanwise film cooling effectiveness results at various locations downstream of the cooling ducts for a) discrete slots, b) round holes, c) pressure side injection, and d) grooved tips (Kim et al., 1995). 38

Figure 2.13 Film-cooling configurations shown a) with a squealer tip (Kwak and Han, 2002b) and b) flat tip (Kwak and Han, 2002a). 39

Figure 2.14 Film cooling effectiveness contours for tip blowing over a flat tip with tip gap 1.5% of the total blade height and blowing ratios of a) M=0.5, b) M=1, and c) M=2 (Kwak and Han, 2002a). 40

Figure 2.15 Film cooling effectiveness contours for tip and pressure side blowing over a flat tip with gap 1.5% of the total blade height and blowing ratios of a) M=0.5, b) M=1, and c) M=2 (Kwak and Han, 2002a). 40

Figure 2.16 Film cooling effectiveness contours for tip blowing over a squealer tip with blowing ratios of a) M=1, and b) M=2 (Kwak and Han, 2002b). 41

Figure 2.17 Film cooling effectiveness for tip and pressure side blowing over a squealer tip with blowing ratios of a) M=1, and b) M=2 (Kwak and Han, 2002b). 41

Figure 2.18 Velocity vectors and magnitudes on the middle plane of tip gap with a gap clearance of 1.5% of the total blade height, turbulence levels of 6.1% for the cases a) without film cooling and b) with film cooling (Acharya et al, 2002). 42

Figure 3-1 Tests were conducted in a low speed wind tunnel. The shaded area is the combustor simulator. 67

Figure 3-2 Static pressure distributions on the shroud a) without a trip wire and b) with a trip wire. 68

Figure 3-3 Schematic of route for secondary air to the microcircuit. 69

Figure 3-4 Picture of the completed test section. 70

Figure 3-5 The test section for the wind tunnel houses three blades, which form two full passages. Flexible walls allow the flow to be adjusted around the test blade in the center. 71

Figure 3-6 Flexible wall adjustment mechanism (FWAM). 71

Figure 3-7 Setting the tip gap. The center blade and baseboard assembly traversed vertically along the threaded rods while gage blocks set the distance for the proper tip gap. 72

Figure 3-8 Four different tip geometries (Hohlfeld, 2003). 72

Figure 3-9 This three-dimensional depiction of the test blade shows the inner components of the dirt purge geometry that was tested in the wind tunnel (Hohlfeld, 2003). 73

Figure 3-10 Negative image of the tip microcircuit geometry from a top view and two isometric views looking at the side from above and below the microcircuit (Hohlfeld, 2003). 73

Figure 3-11 Tip microcircuit numbering scheme for referencing various flow ducts (Hohlfeld, 2003). 74

Figure 3-12 Exit area of each tip microcircuit and dirt purge hole when compared to the entire coolant flow area (Hohlfeld, 2003). 74

Figure 3-13 Comparison of flow distribution within the microcircuit. Numbers 1-16 represent the microcircuit holes with 17 and 18 the dirt purge holes (Hohlfeld, 2003). 75

Figure 3-14 Models of the a) air passage piece and b) outer mold for the blade tip (Santeler, 2002). 75

Figure 3-15 Two part outer mold assembly. Holes that were drilled to leak off excess foam are circled in yellow. 76

Figure 3-16 Final product of foam mold process. 76

Figure 3-17 Final alumina tip model. 77

Figure 3-18 a) Horizontal and vertical velocity profiles measured upstream of the test section. b) Laser Doppler Velocimeter measures the z and x components of flow velocity upstream of the test section. 78

Figure 3-19 a) Vertical velocity profiles for four different dilution mass flow ratios and b) corresponding turbulence levels. 79

Figure 3-20 a) Horizontal profile of the cross-stream velocity component normalized by the free-stream mean velocity direction (w/Uavg) and the free-stream velocity component normalized by the free-stream mean velocity (u/Uavg) for 4.3% dilution flow. b) Horizontal profile of averaged turbulence levels (Tu), turbulence levels based on stream-wise fluctuations (Tu_u), and turbulence levels based on cross-stream fluctuations (Tu_w) for 4.3% dilution flow. 80

Figure 3-21 a) Vertical profile of the cross-stream velocity component normalized by the free-stream mean velocity direction (w/Uavg) and the free-stream velocity component normalized by the free-stream mean velocity (u/Uavg) for 4.3% dilution flow. b) Vertical profile of averaged turbulence levels (Tu), turbulence levels based on stream-wise fluctuations (Tu_u), and turbulence levels based on cross-stream fluctuations (Tu_w) for 4.3% dilution flow. 81

Figure 3-22 Side view of test section showing pitot probe location used to measure inlet velocity profiles. Dynamic pressure was measured at seven equally spaced locations in the y-direction.....82

Figure 3-23 Sample of a horizontal velocity profile at the test section inlet. The dashed line is the mean velocity. 83

Figure 3-24 Static pressure tap configuration for pressure measurements on the shroud and midspan pressure measurements on the blade. 84

Figure 3-25 Static pressure tap array on the shroud overlaying shroud static pressure contours. The locations of the taps are indicated with red dots which were grouped around static pressure gradients (Christophel, 2003). 85

Figure 3-26 Static pressure tap locations on the blade midspan (Christophel, 2003). 86

Figure 3-27 Comparison of experimental midspan pressure distribution to computational predictions. 86

Figure 3-28 Scanivalve wafer and box (Vakil, 2002). 87

Figure 3-29 Transducer box (Vakil, 2002). 87

Figure 3-30 Infrared camera. 88

Figure 3-31 ZnSe window configurations to image blade tip. 88

Figure 3-32 Infrared camera imaging the blade tip. 89

Figure 3-33 An infrared camera image of the alumina tip before any post processing. 89

Figure 3-34 Marker and thermocouple locations for a) foam tip and b) alumina tip. The dashed lines show the areas that are imaged through the ZnSe windows. 90

Figure 3-35 Layout of a thermocouple constructed from flat ribbons of chromel and constantan. 90

Figure 3-36 Repeatability results for adiabatic effectiveness. Tests were run with a large tip gap with 1.0% blowing from the microcircuit and dirt purge holes. 91

Figure 3-37 Lateral averages of the repeatability results for adiabatic effectiveness with a large tip gap at 1.0% blowing from the microcircuit and dirt purge holes. 92

Figure 3-38 Repeatability results for pressure distribution on the shroud. Tests were run with a large tip gap with no blowing. 92

Figure 4-1 Geometric terminology for a turbine blade. 115

Figure 4-2 Two different designs for a turbine blade tip cross-section with the high-speed (engine) blade shown in blue and the low-speed (experimental) blade shown in red (Praisner, 2002). 116

Figure 4-3 Shroud pressure distributions with a flat blade for a) a small tip gap and b) a large tip gap. 116

Figure 4-4 Shroud pressure distribution contours for a large tip gap at a) the baseline (flat tip) case, and at dirt purge blowing ratios of b) 0.10%, c) 0.19%, d) 0.29%, and e) 0.38%. 117

Figure 4-5 Shroud pressure distribution contours for a small tip gap at a) the baseline (flat tip) case and at dirt purge blowing ratios of b) 0.10%, c) 0.19%, d) 0.29%, and e) 0.38%. 118

Figure 4-6 Cross section of the dirt purge cavity showing velocity vectors of coolant flows for a small tip gap with 0.29%

blowing (Hohlfeld, 2003). The black line on the gray blade shape indicates the section plane location. 119

Figure 4-7 Large tip gap adiabatic effectiveness contours with dirt purge hole blowing ratios of a) 0.10%, b) 0.19%, c) 0.29%, and d) 0.38%. 119

Figure 4-8 Small tip gap adiabatic effectiveness contours with dirt purge hole blowing ratios of a) 0.10%, b) 0.19%, c) 0.29%, and d) 0.38%. 120

Figure 4-9 Scheme for lateral averaging of effectiveness values. A MATLAB code sliced the effectiveness data into thin areas normal to the flow and plotted the average effectiveness of each area against the x-direction. 120

Figure 4-10 Laterally averaged adiabatic effectiveness at four dirt purge hole blowing ratios with a large tip gap plotted along the x-direction normalized by the axial chord length. The vertical dashed lines indicate the locations of the dirt purge holes. 121

Figure 4-11 Laterally averaged adiabatic effectiveness at four dirt purge hole blowing ratios with a small tip gap plotted along the x-direction normalized by the axial chord length. The vertical dashed lines indicate the locations of the dirt purge holes. 122

Figure 4-12 Adiabatic effectiveness averaged over the entire tip plotted against blowing ratio for a large and a small tip gap with blowing from the dirt purge only. 123

Figure 4-13 Shroud pressure distribution contours for a large tip gap at a) the baseline (flat tip) case, and at microcircuit blowing ratios of b) 0.5%, c) 1.0%, d) 1.5%, and e) 2.0%. 124

Figure 4-14 Shroud pressure distribution contours for a small tip gap at a) the baseline (flat tip) case, and at microcircuit blowing ratios of b) 0.5%, c) 1.0%, d) 1.5%, and e) 2.0%. 125

Figure 4-15 Tip adiabatic effectiveness contours for a large tip gap at microcircuit blowing ratios of a) 0.5%, b) 1.0%, c) 1.5%, and d) 2.0%. The black arrows label the locations of the microcircuit exits on the pressure side of the blade. The arrows in the 0.5% blowing case are numbered according to the scheme for the microcircuit and dirt purge exits that was laid out in Chapter 3. 126

Figure 4-16 Tip adiabatic effectiveness contours for a small tip gap at microcircuit blowing ratios of a) 0.5%, b) 1.0%, c) 1.5%, and d) 2.0%. 127

Figure 4-17 Laterally averaged adiabatic effectiveness at four microcircuit blowing ratios with a large tip gap plotted along the X-direction normalized by the axial chord length. The vertical dashed lines indicate the locations of the dirt purge holes. 128

Figure 4-18 Laterally averaged adiabatic effectiveness at four microcircuit blowing ratios with a small tip gap plotted along the X-direction normalized by the axial chord length. 129

Figure 4-19 Laterally averaged adiabatic effectiveness with a large tip gap comparing a) 1.0% microcircuit with dirt purge blowing to 0.19% dirt purge only blowing and b) 1.5% microcircuit with dirt purge blowing to 0.29% dirt purge only blowing. 130

Figure 4-20 Laterally averaged adiabatic effectiveness with a small tip gap comparing a) 1.0% microcircuit with dirt purge blowing to 0.19% dirt purge only blowing and b) 1.5% microcircuit with dirt purge blowing to 0.29% dirt purge only blowing. 131

Figure 4-21 Adiabatic effectiveness averaged over the entire tip for all cases with dirt purge blowing only and with combined dirt purge and microcircuit blowing. 132

Figure 4-22 Tip cooling effectiveness contours for a large tip gap at microcircuit blowing ratios of a) 0.5%, b) 1.0%, c) 1.5%, and d) 2.0%. 133

Figure 4-23 Tip cooling effectiveness contours for a small tip gap at microcircuit blowing ratios of a) 0.5%, b) 1.0%, c) 1.5%, and d) 2.0%. 134

Figure 4-24 Laterally averaged cooling effectiveness for large tip gap at four microcircuit blowing ratios. 135

Figure 4-25 Laterally averaged cooling effectiveness for a small tip gap at four microcircuit blowing ratios. 136

Figure 4-26 Area averaged cooling effectiveness plotted against blowing ratio for two tip gap sizes. 137

Figure A-1 T6 Aluminum Block Schematic. 147

Figure A-2 T6 Aluminum Male Hinge Schematic. 148

Figure A-3 T6 Aluminum Female Hinge Schematic. 149

Figure E-1 Top view of the lexan shroud with machined slot for window and lid. 155

Figure E-2 Section view of the lexan shroud. 156

Figure E-3 Lexan filler lid to seal space not occupied by the IR window and frame. 156

Figure E-4 Aluminum frame for housing two 10 mm thick, 6 in x 6 in ZnSe windows. 157

Figure G-1 Heat transfer coefficient ratio contours for a large tip gap. 161

Figure G-2 Heat transfer coefficient ratio contours for a small tip gap. 162

Chapter 1: Introduction

The first patent for a gas turbine design was granted in 1791 to an English colliery manager named John Barber. His design used a chain-driven, reciprocating compressor and a combustion chamber to turn a turbine. This was originally intended to power a horseless carriage, but since its conception variations on his design were developed in which the turbine rotation is used to do some sort of work. One of the more significant advances was the development of the jet engine. Intended to power an aircraft, a jet engine uses a gas turbine to accelerate air and produce a thrust. During the 1930's, Dr. Hans von Ohain of Germany and Sir Frank Whittle of England each patented a jet engine design based on the Brayton cycle. Their designs came to fruition during World War II when von Ohain's engine powered the first flight of the HE178 in 1939. Whittle's engine powered the first flight of the Pioneer jet in 1941 (http://inventors.about.com/).

Figure 1-1 shows a cutaway of Whittle's jet engine design. In a basic turbojet engine, air enters the engine and passes through the compressor where it is pressurized and then mixed with fuel. The fuel burner ignites the high-pressure mixture of fuel and air causing temperatures above 1500°C in the combustion chamber [Wilson and Korakianitis, 1998]. This hot, fast-moving air then enters the turbine section, where stationary vanes direct the air into a turbine wheel like the one pictured in Figure 1-2. The turbine is turned as the hot air flows around the turbine blades. The turbine wheel turns the shaft that is connected to the compressor so that the cycle continues. After passing through the turbine, hot air accelerates through the nozzle and exits the engine. The overall acceleration of air causes a thrust force on the engine in the direction opposite the airflow.

In addition to propulsion, the gas turbine is currently used for power generation. In power generation, the engine operates in a similar manner with the main difference being that as much work as possible is extracted from the turbine. Therefore, no thrust is developed.

In either the propulsion or the power generation industry, the maximum temperature achieved during combustion governs engine efficiency, so the materials in the combustor and turbine are constantly being pushed to the limit. The turbine blades, in

particular, are exposed to some of the hottest temperatures in the engine. Figure 1-3 shows the damage a turbine blade can incur after over 8,000 hours of operation. Researchers try to either find materials that are more temperature resistant and that have higher melting points, develop coatings to protect the materials, or create effective ways to cool these parts.

Figure 1-4 shows the basic setup of a turbine blade and stator vane. Located just upstream of the turbine blades, stator vanes are stationary blades that direct combustor flow to the proper angle of attack for the turbine. Turbine blades are characterized by a concave surface called the pressure side, and a convex surface called the suction side. As the names indicate, there is a pressure distribution around the blade such that the static pressure is lower on the suction side and higher on the pressure side. Hot gas from the combustor flows around the blade, and the pressure difference between the pressure and suction sides drives the rotation of the turbine wheel.

Pending the advent of some new high temperature materials, turbine blade temperatures must be maintained below the material melting point through advanced cooling techniques. Air from the compressor is cool relative to the air temperature in the combustor, and some of this air can be redirected to cool the turbine blades rather than pass through the combustor. Figure 1-5 illustrates currently used methods of cooling a blade, so the engine can operate at higher temperatures. The first is through film cooling techniques which protect the external surfaces of the blade from the hot gases of the combustor. By injecting air diverted from the compressor into the mainstream flow through strategically located holes, a layer of cool air can be formed around the blade. A number of factors go into just how effectively the outer blade is cooled such as the location and shape of the hole and the blowing ratio. Hole location and shape determine the areas of the blade that are cooled and how well the coolant spreads upon injection. The blowing ratio is a measure of the mass flux of the injected coolant in relation to that of the mainstream flow. Generally, film cooling is improved with higher blowing ratios. However, the blowing ratio could be so large that coolant is lifted off the blade surface into the mainstream flow, so that no cooling is gained.

Another method of blade cooling is through internal convective cooling, which occurs inside the blade as shown in Figure 1-5b. Heat conducted through the blade walls

can be removed through serpentine passages inside the blade. A third form of blade cooling is impingement, shown in Figure 1-5c. Impingement builds off of convective cooling techniques by modifying internal passages to accelerate cool air through small holes. The jet of air created by the smaller flow area impinges upon the inside blade wall resulting in localized cooling. This method can be used to cool spots that get particularly hot. Figure 1-6 shows a modern multi-pass turbine blade that incorporates film cooling, convective cooling, and impingement cooling.

In a simple case with no film-cooling, the turbine blade can be reduced to the simple one-dimensional heat transfer scenario shown in Figure 1-7. A material with thickness, t, represents the blade wall that is exposed to hot air flow on one side and cool air flow on the other. The resulting heat transfer, Q, is passed through the material from the hot side to the cool side. The heat transferred from the hot flow to the blade surface is described as

$$Q = h_g A_g \left(T_g - T_{s1}\right) \tag{1-1}$$

where h_g is the external heat transfer coefficient, A_g is the effective external area, T_g is the gas path temperature, and T_{s1} is the external wall temperature. Film cooling techniques inject cool air into the hot side to replace the hot mainstream flow with coolant or at least reduce the local temperature of the flow. Here, the aim is to reduce the heat transferred to the wall by minimizing the difference between T_g and T_{s1}. However, the injected coolant alters the gas path temperatures when it mixes into the hot flow as shown in Figure 1-8. This means that the gas path temperature cannot be considered uniform along the wall, and a temperature distribution is needed to describe the mixture of T_c and T_g. Temperature measurements on the surface of an adiabatic wall, T_{aw}, with film cooling can provide an accurate depiction of the local temperatures because the temperature on the adiabatic surface is the temperature of the flow immediately adjacent to the surface. If adiabatic wall temperatures are used to represent the gas path temperatures with film cooling, then the heat transferred from the flow to the blade surface can be rewritten as

$$Q = h_g A_g \left(T_{aw} - T_{s1}\right) \tag{1-2}$$

With internal convection, the aim is to remove as much heat from the wall as possible by maximizing Q. Heat transfer through the inside wall is described as

$$Q = h_c A_c \left(T_{s2} - T_c \right) \qquad (1\text{-}3)$$

where T_{s2} is the internal wall temperature, h_c is the internal heat transfer coefficient, A_c is the internal heat transfer area, and T_c is the coolant temperature. To maximize the heat removed from the blade wall, turbine blade designers look for ways to maximize h_c which is a function of the flowfield and the working fluid (air) properties. The turbulence promoters depicted in Figure 1-6 are variations in the blade wall geometry designed to increase the internal heat transfer coefficient. It would also be desirable to maximize the temperature difference between the internal wall temperature and the coolant temperature. The coolant temperature is fixed by compressor conditions and cannot directly be altered in the realm of turbine design. Therefore, the internal wall temperature is determined by conduction from the external wall. To maximize the temperature difference between T_{s2} and T_c, we would want the internal wall temperature to be as high as the external wall temperature. This situation does not exist because of the thermal resistance of the blade wall material. The heat conducted through the blade wall is described as

$$Q = \frac{kA_k}{t} \left(T_{s1} - T_{s2} \right) \qquad (1\text{-}4)$$

where k is the thermal conductivity of the wall and A_k is the effective conduction area. To more efficiently remove heat from the blade, it is beneficial to maximize Q. Equation 1-4 shows that heat transfer is dependent on conductivity and wall thickness. Because wall thickness is in the denominator, heat transfer is increased with a thinner blade wall.

A novel approach to blade cooling that incorporates the previously discussed cooling methods has been developed by Pratt & Whitney. This new design attempts to maximize internal convective cooling by reducing the blade wall thickness and incorporating enhanced film cooling. The design is called a microcircuit and is introduced in more detail in the next section.

In principle, the microcircuit design may extend to cooling the entire turbine blade although this report concentrates on the tip region, that is, the part of the blade radially located furthest from the engine axis. Figure 1-9 depicts how the blade is contained in a shroud, which acts as a duct to direct all flow around the turbine blade. There exists a slight gap between the tip of the blade and the shroud to allow the blades to

rotate. Even in the event of a perfectly constructed turbine-shroud assembly, thermal expansion during transient engine operations causes rubbing to occur between the blade tip and the shroud. This removes material from the blade, leaving a tip gap when the engine returns to steady operation. Typical gap sizes in an engine may range from 0.254 mm to 0.762 mm (0.010 in to 0.030 in), which corresponds to between 1.0% and 1.5% of the entire radial span of the blade. Figure 1-10 shows a simple depiction of a tip gap. This tip gap acts as a sudden flow contraction, and hot gases from the combustor accelerate across this tip gap causing highly turbulent, three-dimensional flows in the tip region. The flow is driven across the tip gap as a result of the inherent pressure difference between the blade's pressure and suction surfaces. The leakage causes heat transfer to the tip that is detrimental to the operation life of the blade and also causes pressure losses that reduce aerodynamic efficiency.

1.1 Microcircuit Description

As discussed previously, Pratt & Whitney developed a new design to cool the tip region of a turbine blade. The design is intended to be used for Pratt & Whitney's F135 aero engine. A microcircuit is a series of passages internal to the blade that eventually exhausts the coolant fluid through film-cooling holes placed on the external blade surface. In this way, a microcircuit makes use of internal convective cooling before supplying flow to external film-cooling. While this may not be a new concept, the manufacturing technology needed to create the small internal passages in the microcircuit has only recently become available. The second aim of the microcircuit/film-cooling design was to reduce flow leakage across the tip with film-cooling injection acting as a flow blockage. The tip leakage has deleterious effects on the operation life of a blade, but this leakage could be reduced with blowing from the microcircuit.

The microcircuit shown in Figure 1-11 is the particular design that was tested in this research. The outer blade shape is a two-dimensional extrusion based on the tip profile from a Pratt & Whitney turbine blade design. The microcircuit passages are fed coolant air from a plenum that is routed just beneath the tip surface towards the pressure side as shown by the simplified section view in Figure 1-12. These internal passages

remove heat from the blade surface through convection. The coolant is then injected into the flow from rectangular hole shapes on the pressure side of the blade. This forms a film of coolant that wraps over the blade tip as a result of the inherent pressure difference between the pressure and suction sides of the tip gap. In this way, the microcircuit provides convective cooling to the external surface.

The dirt purge holes, also shown in Figure 1-11, are a geometry that serves a practical function and are not necessarily intended to serve as a film cooling mechanism. The dirt purge geometry is a result of the need to stabilize the blade when it is being formed in a mold yet also serves to expel dirt from the internal passages of the blade. Dust and dirt particles are drawn towards the tip by centrifugal forces and exit through the dirt purge holes rather than clogging smaller film cooling holes elsewhere on the blade.

1.2 Heat Transfer Analyses of a Turbine Blade with a Microcircuit Design

The ability of the microcircuit to cool the blade can be understood if the temperature is known at all locations within the blade volume. Ultimately, turbine durability engineers are interested in the magnitudes and locations of the highest blade temperatures where they expect degradation to occur. The microcircuit is a complex geometry that poses a serious challenge for heat transfer analysis. Such a complex, three-dimensional problem may be better understood if first investigated with principles of heat transfer in one dimension. According to calculations by Alahyari [2000] and Bogard [2001], if the microcircuit could be compared to the plane wall in Figure 1-7, then Equations 1-2, 1-3, and 1-4 can be combined to describe the heat transferred through the entire blade as

$$Q = h_g A_g \left(T_{aw} - T_{s1}\right) = \frac{kA_k}{t}\left(T_{s1} - T_{s2}\right) = h_c A_c \left(T_{s2} - T_c\right) = \Psi A\left(T_{aw} - T_c\right) \qquad (1\text{-}5)$$

where

$$\Psi A = \frac{1}{\frac{1}{h_g A_g} + \frac{t}{kA_k} + \frac{1}{h_c A_c}} \qquad (1\text{-}6)$$

We can now express these equations in dimensionless terms to solve for the external surface temperature. The normalized temperature of the external wall can be written as

$$\theta = \frac{T_{aw} - T_{s1}}{T_{aw} - T_c} = \frac{\Psi A}{h_g A_g} = \frac{1}{1 + Bi + h_{gc}} \tag{1-7}$$

where the Biot number is

$$Bi = \frac{h_g t}{k} \tag{1-8}$$

and the internal to external heat transfer coefficient ratio is

$$h_{gc} = \frac{h_g}{h_c} \tag{1-9}$$

This implies that the external surface temperature of the blade, T_{s1}, can be solved given the gas path temperature, coolant temperature, and the internal and external heat transfer coefficients. The geometry and composition of the blade should be well known, so the surface areas and thermal conductivity are also known. When the surface temperature is found, the temperature at any point along the wall thickness can be calculated with a simple conduction equation.

This analysis neglects the effects of lateral conduction. At steady-state conditions, the temperature distribution in the actual three-dimensional blade volume with constant thermal conductivity would be derived by solving

$$\frac{\partial^2 T}{\partial x^2} + \frac{\partial^2 T}{\partial y^2} + \frac{\partial^2 T}{\partial z^2} = 0 \tag{1-10}$$

for all locations in the Cartesian space. Finding an exact, analytical solution for the temperature distribution is impractical for a complex geometry like the microcircuit. However, a discrete approximation through finite difference methods is feasible. Blade surface temperatures are required to set boundary conditions to spatially resolve the temperature distribution throughout the blade volume. As revealed in the one-dimensional investigation, surface temperatures can be solved given T_{aw}, T_c, h_g, and h_c at each surface. Distributions of these parameters at each surface of the blade can be used to solve discrete temperature solutions to Equation 1-10.

The research presented in this study was contracted by Pratt & Whitney to provide the boundary conditions on the blade tip surface needed to numerically resolve a

complete blade temperature distribution. Temperature measurements on a large scale blade in a low speed wind tunnel facility are used to calculate heat transfer coefficients. These experimental temperature measurements are reported in dimensionless terms that can easily be related to engine conditions. A description of these terms and how they are used to calculate h_g and h_c is given below.

Due to the film cooling from the microcircuit, the local fluid temperature actually represents a nonuniform mixture of coolant (T_c) and mainstream air (T_g) across the tip surface, as discussed previously. In order to quantify T_{aw}, temperatures were measured on a foam tip with low thermal conductivity. If conduction is absent, then an adiabatic wall condition exists and external measured temperatures represent the local fluid temperature.

Now, similar measurements can be made on a surface of high thermal conductivity that matches the conditions of the actual engine. Because the thermal conductivity of the blade is large, the Biot number decreases and can be dropped from the right hand side of Equation 1-7. Measurements on the conductive surface represent T_{s1}, so h_{gc} can be solved. With the heat transfer coefficient ratio, we need only to find either h_g or h_c, and we will know both coefficients. The present study involved measurements of the adiabatic wall temperature presented nondimensionally as adiabatic effectiveness. Adiabatic effectiveness is defined as

$$\eta = \frac{T_\infty - T_{aw}}{T_\infty - T_c} \tag{1-11}$$

where T_∞ is the freestream temperature. We express η as a dimensionless temperature so that wind tunnel measurements can be correlated to engine conditions, and then T_{aw} can be expressed as an actual engine temperature. This study also presents measurements of overall cooling effectiveness made on a conductive surface with engine matched Biot numbers as

$$\phi = \frac{T_\infty - T_m}{T_\infty - T_c} \tag{1-12}$$

where T_m is the metal temperature on the conductive surface. When T_m is correlated to engine conditions through ϕ, it represents T_{s1}. With experimental values for T_{s1} and T_{aw}, the heat transfer coefficient ratio, h_{gc}, can be solved with Equation 1-7. These

measurements are the extent to which this study contributes to the tip surface boundary conditions.

Another study by Christophel [2003], aims to measure the external heat transfer coefficient, h_g, by introducing a known heat flux, q″, to the adiabatic surface. By making temperature measurements on this wall, h_g can be solved with the area-averaged external convective heat transfer in Equation 1-1 or

$$q'' = h_g\left(T_g - T_{s1}\right) \qquad (1\text{-}13)$$

Finally, h_g can be solved, thus, providing the last boundary condition to solve for turbine blade temperatures. With a proper distribution of the external heat transfer coefficients, the internal heat transfer coefficient, h_c, can be extracted from the coefficient ratio, h_{gc}.

1.3 Research Objectives

The purpose of this research is to obtain distributions of adiabatic effectiveness, overall cooling effectiveness, and the heat transfer coefficient ratio on the tip of a scaled up turbine blade incorporating microcircuit and film-cooling technologies. The blade model was tested in a large scale, low speed wind tunnel where the inlet flow to the blade had a Reynolds number of 2.2 x 10^5 (based on the blade axial chord). There was no relative motion simulated between the blade and shroud. Open literature shows that the tip leakage flow is driven primarily by the pressure-to-suction side pressure difference rather than by rotational effects. Chapter 2 provides a further discussion on this. For four different blowing ratios and two different tip gap sizes, I made spatially resolved temperature measurements at the tip and pressure measurements on the shroud. An additional set of measurements were made to study the cooling effects of the dirt purge holes without the microcircuit.

The next chapter in this thesis presents a review of literature pertaining to the flowfield and heat transfer of the blade tip region. Chapter 3 describes in detail the experimental methods, facilities, and instrumentation involved in this study. Chapter 4 goes on to present the analysis of the results of the data taken during experimentation. Finally, Chapter 5 summarizes the conclusions that were drawn from these results and

offers recommendations for further studies and further improvements to the microcircuit design.

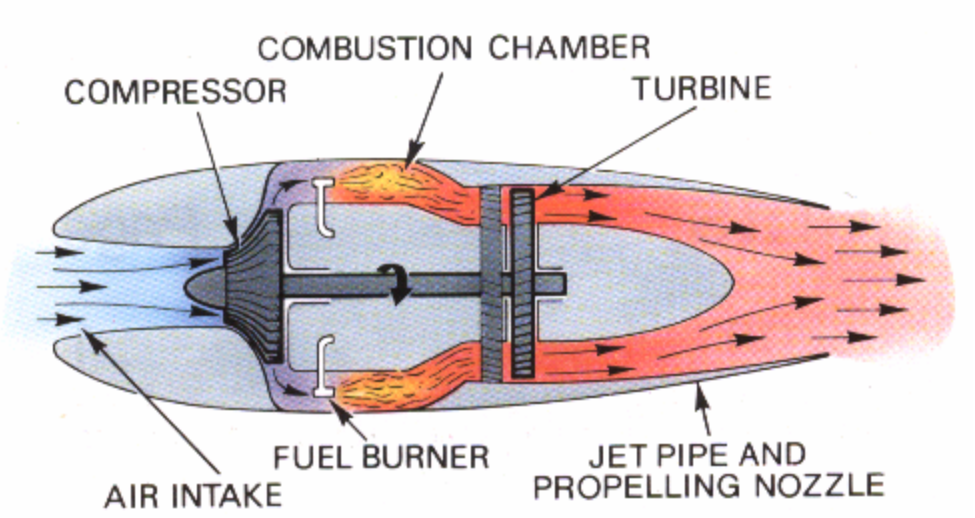

Figure 1-1 Cutaway of a Whittle-type turbo-jet engine (Rolls-Royce, 1992).

Figure 1-2 A turbine wheel with unshrouded turbine blades (*IHPTET: Technology Teams in Action*).

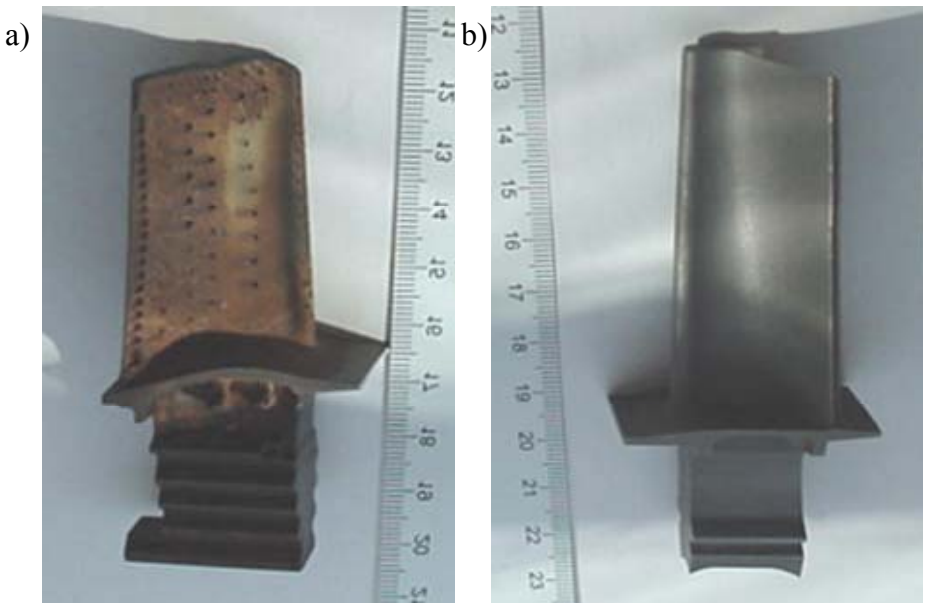

Figure 1-3 A turbine blade a) after operating in a sand laden environment for 8,200 hours and 4,500 flights, and b) before entering an engine and without film cooling holes. Note the scale is in cm. (Blades courtesy of Pratt & Whitney).

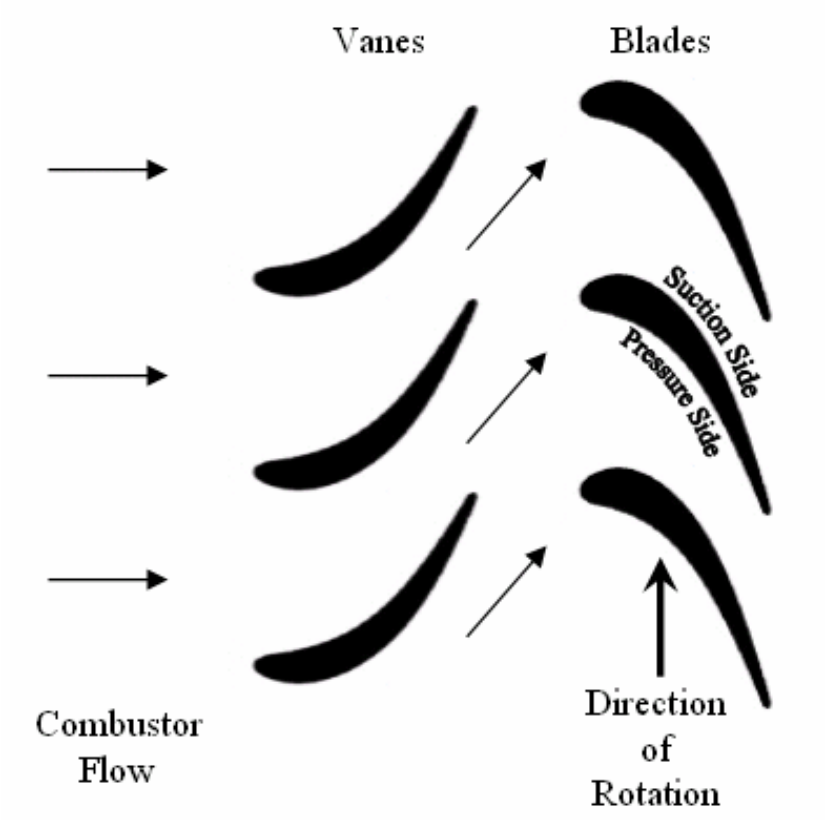

Figure 1-4 Layout of turbine blades and stator vanes.

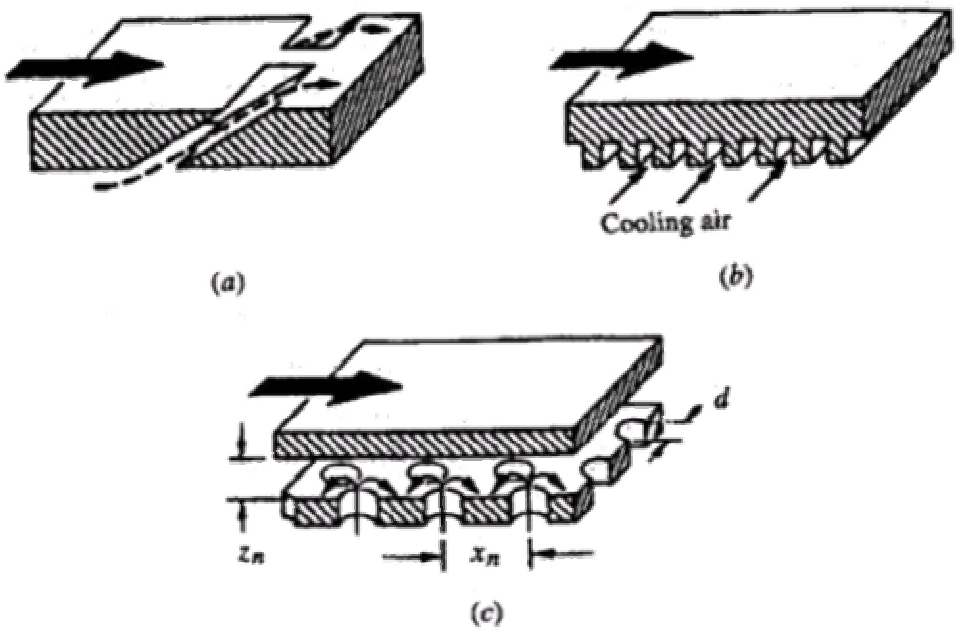

Figure 1-5 Methods of blade cooling are a) film cooling, b) internal convection, and c) impingement (Mattingly, 1996).

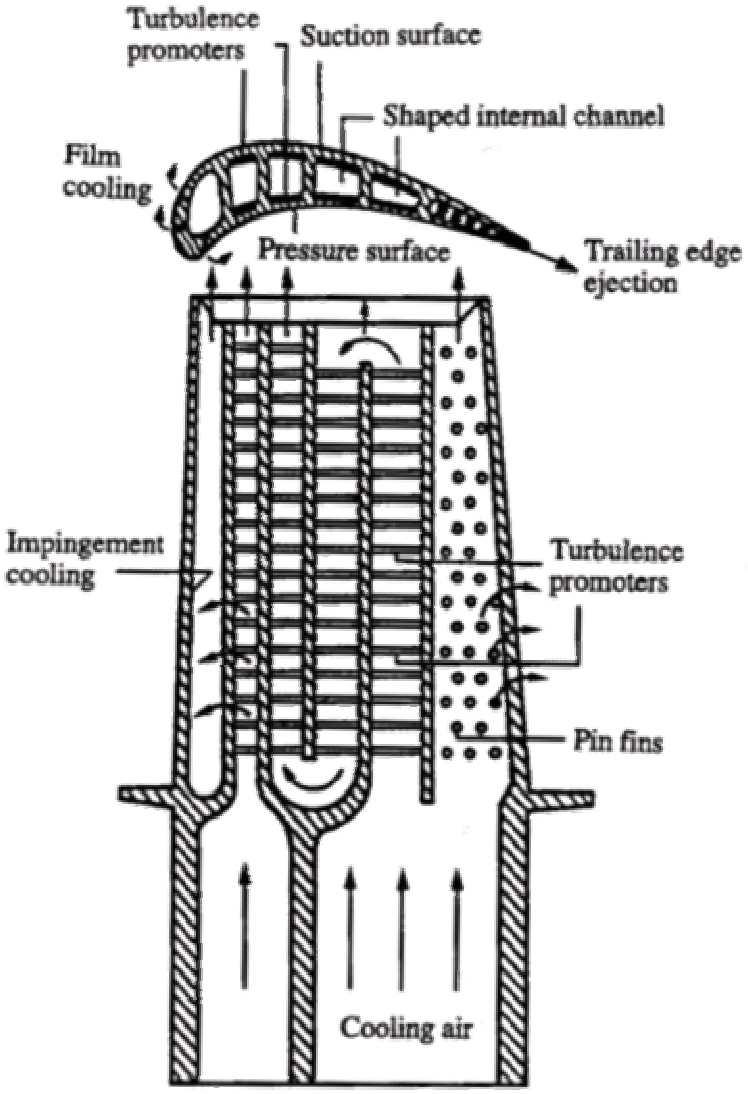

Figure 1-6 A modern multi-pass turbine blade cooling scheme (Han et al., 1984).

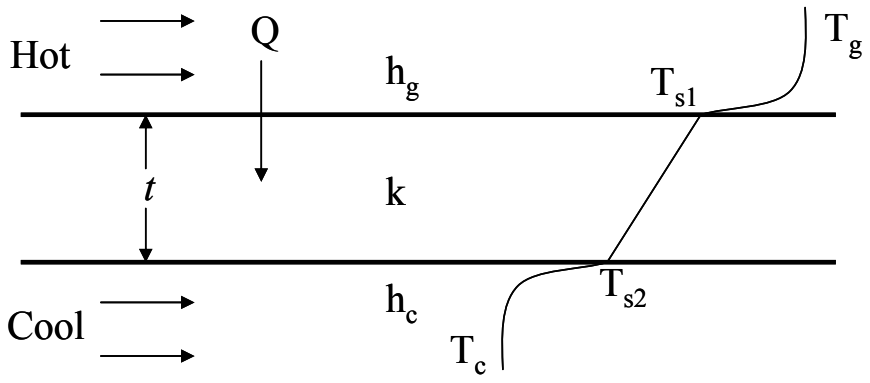

Figure 1-7 Plane wall with fluid movement on both sides.

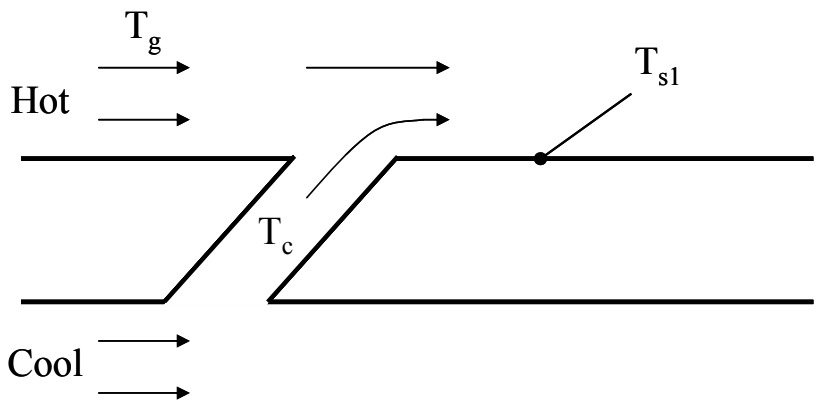

Figure 1-8 Plane wall with film cooling.

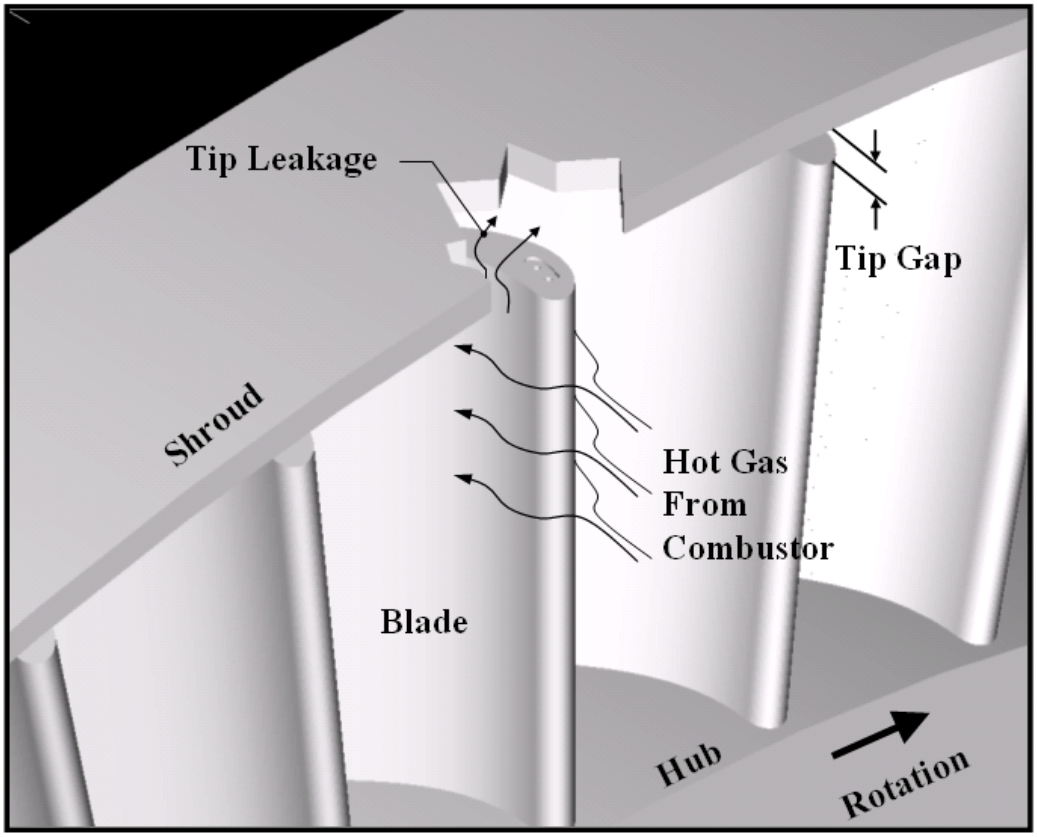

Figure 1-9 Representation of turbine blade tip and shroud orientation with tip leakage.

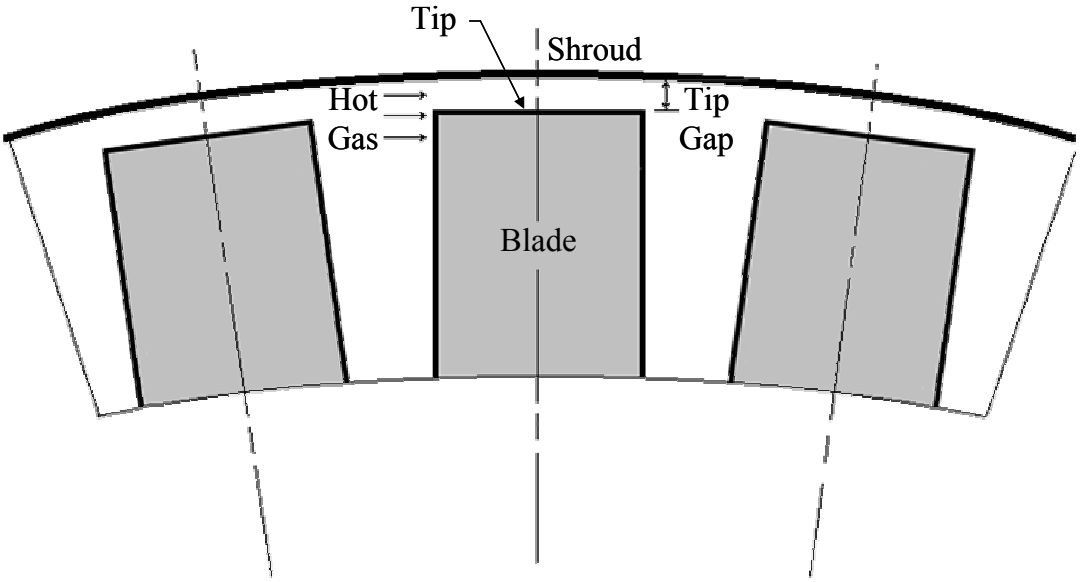

Figure 1-10 Viewed from the direction of the flow, a simplified section of a turbine wheel. Hot gases leak across the gap between the tip and the shroud.

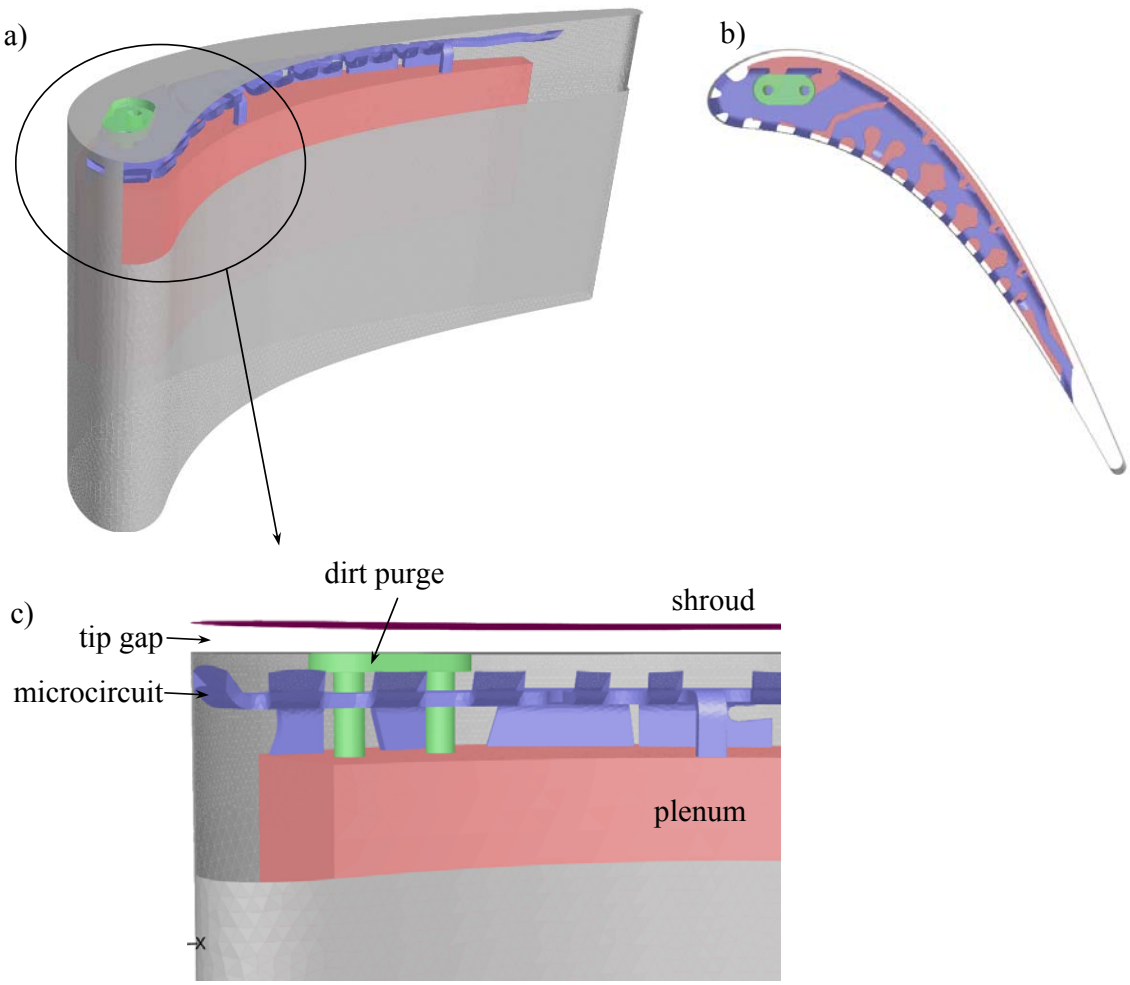

Figure 1-11 The microcircuit geometry that was tested in this study: a) an isometric view of the blade with part of the blade removed to show the air passages; b) a top view with the tip surface removed; c) a closer view detailing the dirt purge holes in green and the microcircuit passages in blue. Coolant to the dirt purge and microcircuit was supplied by the plenum shown in red (Hohlfeld, 2003).

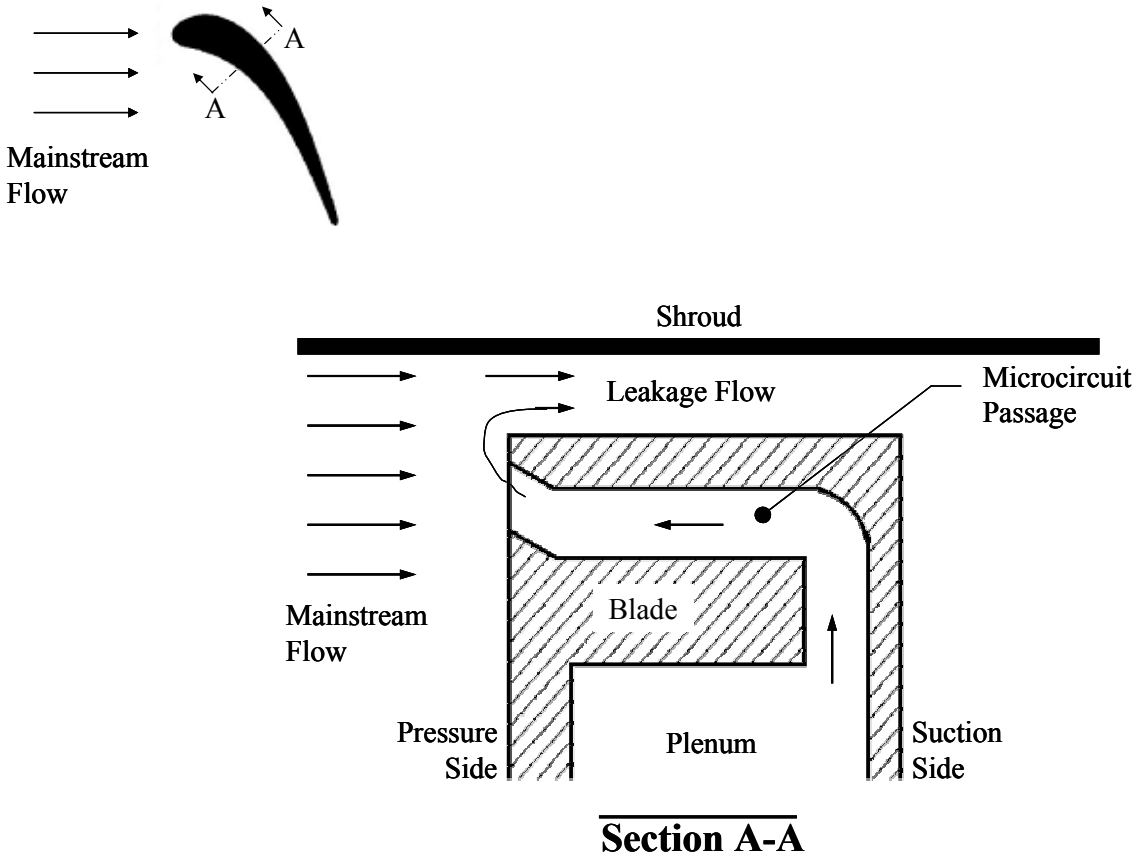

Figure 1-12 Section view of a microcircuit passage.

Chapter 2: Review of Relevant Literature

Studies on the tip region of a turbine blade have been ongoing for the past fifty years. Bunker [2000] provides an overview of research in this area. He attributes the earliest studies on tip flows to Allen and Kofskey [1955] and the work they did to observe secondary flows in the tip region through smoke visualization in a rotating turbine rig. Since then, numerous studies have examined the flowfield in the tip region, while heat transfer on the tip has been under scrutiny for the past twenty years.

This chapter presents key studies concerned with the tip region of a turbine blade. Because this thesis presents results from a stationary blade cascade, the first section of this chapter highlights some of the studies carried out in rotating and non-rotating rigs. By showing that relative motion between the blade and shroud has negligible effects on the flow and heat transfer in the tip region, these studies verify the results presented later. The second section provides an overview of the numerous aerodynamic studies, which leads to a discussion of the flow models that have been observed in and around the tip gap. The next section will describe studies done to observe heat transfer in the tip region. Some studies vary tip geometries while others observe the effect of tip injection schemes. A general understanding of past research should serve to highlight the uniqueness of this study and how it adds to the current knowledge base of tip heat transfer.

2.1 Effects of Relative Motion Between the Tip and Shroud

Studies observing the tip region have been carried out in experimental facilities that simulate blade rotation and others that house blade cascades which are stationary relative to the shroud. With their pressure measurements on a tip gap in an annular turbine cascade, Morphis and Bindon [1988] assert that the flow across the tip gap is driven by the inherent pressure difference across the blade. The flow effects of rotation were found to be minor in comparison. Studies presented later in this chapter find that tip leakage flow causes a vortex on the suction side of a blade. Lakshminarayana, et al. [2000] found that the overall behavior of this tip leakage vortex and the associated aerodynamic loss in a rotating rig are very similar to those observed in a static cascade.

As with tip flows, heat transfer at the tip is mainly influenced by the pressure driven leakage. Mayle and Metzger [1982] completed the first study aimed at heat transfer in the tip region. They found heat transfer coefficients on flat tip models for various flow Reynolds numbers and rotational speeds. This study showed average tip heat transfer was a weak function of rotational speed and was influenced most by pressure driven flow across tip. In another study with a shroud surface moving over a simple rectangular cavity, Chyu et al. [1989] also determined that the relative motion of the blade and shroud had little influence on tip heat transfer.

A recent study by Srinivasan and Goldstein [2003] used the rig shown in Figure 2-1 to study how the relative motion between the shroud and tip affected tip heat transfer. Napthalene sublimation techniques were used to measure heat transfer on the tip surface at five tip gap sizes. The results were expressed as Sherwood numbers and revealed negligible measured effects of relative motion in all cases except at a gap size of 0.86% of the chord. At the 0.86% case, there was an increase in Sherwood number near the trailing edge. This and other studies have shown that tip flows are primarily determined by the pressure difference from pressure side to suction side while blade motion relative to the shroud is less influential.

2.2 Tip Leakage Flow Models

Since fluid movement directly affects heat transfer, it is important to understand the nature of the flow around a turbine blade tip. Spurred by efforts to improve aerodynamic efficiency, much work has already been done to observe flowfields around a turbine blade. Tests have been carried out via computational methods and experimental methods such as large scale blade models in low speed wind tunnels. Morphis and Bindon [1988] used flow visualization to show the presence of a gap separation bubble on a blade tip with a sharp edged perimeter. However, the addition of a rounded edge perimeter eliminated this bubble.

A later study performed by Bindon [1989] on a linear cascade of flat tipped blades revealed some general flow characteristics of the tip region. By making pressure

measurements in and around the tip gap, Bindon calculated gap discharge coefficients to describe the modes of tip loss. Possible modes included internal gap loss, suction corner mixing loss, and endwall/secondary loss. Internal gap loss is caused by friction effects inside the tip gap and was determined to comprise 39% of the total loss. Endwall/secondary losses from skin friction shear stress on the fluid flow moving across the walls contributed 13% of the total loss. Mixing losses are incurred when flow exits the gap to mix with the mainstream flow. Mixing is of particular interest because it is responsible for the remaining 48% of the total loss.

Bindon depicts a model of the tip gap flow as shown in Figure 2-2. Again, a separation bubble of circulating air is thought to form along the pressure side of the tip as mainstream air leaks into the tip gap. This bubble grows along the blade chord until it separates and is forced across the tip with the pressure driven leakage flow near mid-chord. As this leakage flow exits the tip gap, it collides with the mainstream flow which has a different velocity magnitude and direction. This causes a large tip leakage vortex off the trailing edge of the blade's suction side. Yamamoto [1989] studied a cascade with tip clearance in a low speed wind tunnel to quantify losses near the tip region. He also observed a tip leakage vortex caused by leakage across the rear part of the tip gap and determined that it was influenced by incidence angle and tip clearance size.

Prasad [1999] suggests that this tip leakage vortex could be diminished with flow injection along the pressure side of the blade tip shown in Figure 2-3. A weaker vortex could result in reduced aerodynamic losses caused by mixing with the mainstream. With testing done in a large scale rotating rig, he measured static pressures on the shroud and total pressures in a plane at the blade exit in cases with and without blowing. In tests without blowing, pressure contours on the shroud revealed a tip leakage vortex and a separation bubble along the pressure side of the tip, which further verifies past studies. This separation bubble is said to cause a *vena contracta* as flow enters the tip gap. Effects of the *vena contracta* and the tip leakage vortex can be seen in the pressure coefficient contours in Figure 2-4. In tests with blowing, he showed that aerodynamic losses associated with the tip leakage vortex were diminished as the injected flow reduced the mass flow rate of the fluid that leaks over the tip. Prasad [1999] concludes that turbine efficiency could be improved by as much as 0.8% with pressure side flow injection.

2.3 Tip Heat Transfer Studies

Researchers have not considered heat transfer on a turbine blade tip for as long as they have considered aerodynamics at the tip. However, the complex three-dimensional flows in the tip region make it a troublesome area for durability engineers. Hot gas from the mainstream flow accelerates across the tip gap causing increased heat transfer and reducing the blade's operation life. Heat transfer analysis at different tip geometries or with film cooling can lead to better blade design. Here, we present a review of literature regarding heat transfer on geometries without injection, with particular attention paid to squealer geometries. Finally, studies regarding tip heat transfer with tip injection are discussed.

No Blowing. The first study that measured spatially resolved tip heat transfer coefficient distributions in detail was carried out by Bunker et al. [2000]. For sharp edged tips and rounded edge tips, heat transfer measurements were made on a linear blade cascade using a liquid crystal method that is based on hue detection. Also, pressure distributions were measured on the shroud and the tip surface with a sharp edged tip. Pressure measurements agreed well indicating similar local characteristics in the tip clearance. The heat transfer distributions on the tip surface revealed an interesting trend for all cases. Shown in Figure 2-5, a region of low heat transfer, or "*sweet spot*," on the mid-chord section of the tip was apparent for all tip clearances and edge types. This study also showed that a small edge radius allows greater tip leakage flow than a sharp edge causing an increase in heat transfer of about 10% when compared to the sharp edge tip. Likewise, larger tip clearances allowed more leakage flow increasing tip heat transfer coefficients. In a parallel study, Ameri and Bunker [2000] present computational predictions for convective heat transfer coefficients on flat turbine blade tips with sharp edges and with round edges. Overall, they determined that the calculated tip heat transfer agreed well with the experimental results, but the rounded edge blade compared better than the sharp edge blade. The absence of separation on the rounded edge may contribute to the better agreement.

In addition to flat tips, studies have been carried out on numerous tip geometries. Many heat transfer studies have concentrated on squealer geometries in which the material around the perimeter of the blade is raised to reduce heat transfer on the tip surface while protecting the tip from rubbing against the shroud.

Yang et al. [2002] reported computational predictions of heat transfer coefficients on flat blade and squealer blade tips with different turbulence models. The highest leakage flow velocity and, hence, the highest heat transfer coefficients occurred at mid-chord on the pressure side. Further verifying the results in Bunker et al. [2000], a low heat transfer region or "*sweet spot*" was observed near the leading edge of the blade. Also, vortex roll-up along the suction side was initiated near the location of maximum blade thickness, which indicated the presence of a tip leakage vortex.

Papa et al. [2003] performed experimental flow visualization and heat transfer studies on blade tips with squealer geometries and winglet geometries. The winglet geometry, shown in Figure 2-6, has a wall on the suction side much like a squealer tip. The main difference between the two designs is the protruding winglet on the pressure side. Flow visualization was done with an oil dot technique on the tip, and heat transfer coefficients were acquired with a naphthalene sublimation technique. They observed higher heat transfer with the squealer as tip gap increased, but the clearance was less influential with the winglet. Another result of increasing the tip clearance is that the exit location of the leakage flow moves back towards the trailing edge.

Experimental squealer studies by Bunker and Bailey [2000] showed how squealer depth and tip clearance impact turbine blade tip heat transfer. As in Bunker et al. [2000], a hue detection liquid crystal method was used to measure heat transfer coefficients. Generally, increasing the squealer cavity depth resulted in lower heat transfer coefficients on the tip. It was also shown that tip clearance affected heat transfer on a squealer less than on a flat, sharp edged blade tip.

Tip Injection Studies. If the wealth of studies on tip heat transfer is limited when compared to that on tip flow models, there is even less literature that focuses on heat transfer with blowing.

Kim and Metzger [1995] studied the effects of film cooling on a simulated tip gap. They used the rectangular airfoil depicted in Figure 2-7 rather than a blade geometry. The test layout shown in Figure 2-8 used liquid crystal coatings and a computer vision system to determine heat transfer coefficients and effectiveness on the tip. This setup operated on the principle that the tip leakage is mostly driven by the pressure-to-suction side pressure difference and is nearly independent of rotational effects. Tests were conducted with three different mainstream Reynolds numbers ($15x10^3$, $30x10^3$, and $45x10^3$ based on hydraulic diameter) and with two tip clearances at gap height-to-slot width ratios of 1.5 and 2.5. Blowing ratios were also varied from M = 0.01, 0.3, 0.5, and 0.9. Their study indicated that significant protection from convective heat transfer to the tip can be gained with film injection from the pressure side.

Figure 2-9a shows effectiveness distributions for one case across the span of the blade for different locations downstream of the slots. At about one slot width downstream of the cooling slots, effectiveness levels are highest behind the slots, but between the slots they drop by as much as 50%. This variation decreases further downstream as the injected air mixes with the leakage air. The spanwise spacing of the slots is such that there are no regions with zero-effectiveness levels after one slot width downstream of injection. Figure 2.9b shows spanwise averaged effectiveness plotted for the three Reynolds numbers at a blowing ratio of M=0.5 with the larger tip gap. Effectiveness varies considerably with blowing ratio but does not appear to change as much with the Reynolds number. The strong influence of blowing ratio on effectiveness can be seen in Figure 2.10 where blowing ratio is varied for three different Reynolds numbers. Downstream of the coolant injection, spanwise averaged effectiveness levels improve as the blowing ratio increases.

Kim et al. [1995] summarized Metzger's work on tip heat transfer and film cooling, which involved a variety of tip shapes and coolant injection configurations with simplified rectangular sections. The experimental setup and procedure are similar to those in Kim and Metzger [1995] though the four injection geometries shown in Figure 2-11 were tested. The geometries included discrete slots on a flat tip from Kim and Metzger [1995], round holes on a flat tip, round holes on a grooved or squealer tip, and flared slots on the pressure side wall. As before, film effectiveness measurements were made on two

tip gap clearances at different blowing ratios and different mainstream Reynolds numbers.

Figure 2-12 shows spanwise effectiveness levels at four locations downstream of the coolant injection for the four different geometries. All cases shown are at the same mainstream Reynolds number, tip clearance, and injection blowing ratio. The results for the discrete slot are similar to those in Kim and Metzger [1995] with the highest effectiveness in line with the slots. The round hole results in Figure 2-12b show lower effectiveness levels and less defined peaks downstream of the round hole locations as compared with the other hole geometries. There seem to be six peaks in effectiveness with two corresponding to each hole location. This result, coupled with the apparent increased mixing between secondary and leakage flows, indicates the presence of a horseshoe-type vortex at each hole. The effectiveness levels for pressure side injection, shown in Figure 2-12c, are about the same magnitude as the round hole case, but with more spanwise variation for all downstream locations on the tip. Although not evident from the effectiveness measurements, convective heat transfer measurements indicate coolant separation on the upstream corner of the tip. For this reason, increased blowing from the pressure side injection slots does not necessarily improve cooling as is indicated with the other three geometries. A higher blowing rate may cause the coolant to reattach farther downstream causing a larger uncooled portion of the tip. Of the four geometries, the round holes on the squealer tip showed the lowest cooling levels. From these results, it is important to note that there were no uncooled regions measured downstream of any coolant injection and that, with the exception of the pressure side injection case, increased blowing rates lead to better cooling.

Using the transient liquid crystal technique, Kwak and Han [2002a,b] performed two studies measuring heat transfer coefficients and cooling effectiveness on a large scale blade with film cooling. The first study concentrated on a flat tip blade with blowing [2002a], and the second study compared those results to a squealer tip with blowing [2002b]. As diagramed in Figure 2-13, film cooling holes were placed on the tip and on the pressure side wall near the tip of a flat blade and a squealer blade. Unlike the rectangular sections used by Kim et al. [1995], the blade profile in this study was an

aircraft turbine blade profile. For both the flat blade and the squealer blade, three different tip gap sizes were tested at three different blowing ratios.

Figure 2-14 shows the effectiveness contours for three blowing ratios on a flat blade tip with coolant being released from the tip only. In the color scheme for these effectiveness contours, low cooling levels are depicted with blue and high cooling levels are red. Note that this color scheme will be reversed for the results provided later in this paper. With increased blowing ratio, there is increased cooling with a maximum effectiveness of 0.2. However, the cooled regions are limited to the areas immediately downstream of the injection holes. Figure 2-15 shows the same cases with the addition of blowing from the pressure side wall. Again, with increased blowing ratio comes increased film cooling although at the lowest blowing effects of the pressure side cooling are hardly detectable. For the highest blowing ratio, the pressure side holes contribute significant cooling at the trailing edge as coolant flow accumulates.

The presence of the squealer geometry dramatically changes flow across the tip. Figure 2-16 shows effectiveness contours for a squealer tip with tip blowing only at the same tip gap and blowing rates as the flat tip shown in Figure 2-14. Because of the circulating flow inside the squealer cavity, coolant from the tip blowing flows toward the pressure side instead of flowing towards the suction side with the pressure driven leakage across a flat tip. Cooling levels on the squealer tip are higher than they were for the flat tip, with the highest levels of 0.35 occurring near the holes at the upstream portion of the blade tip. Effectiveness increases dramatically at the trailing edge when blowing is added at the pressure side wall near the tip. Figure 2-17 shows the contours that are comparable to the flat tip case in Figure 2-15. As with the flat tip, the highest cooling area occur near the trailing edge as coolant accumulates there. Some areas of the pressure side rim were cooled by the pressure side blowing, but some of the coolant passes over the cavity to the suction side rim without cooling the tip surface. Kwak and Han concluded that increased blowing ratio caused increased film cooling effectiveness for all cases. It was shown that the pressure side injection acted as a flow resistance for the tip leakage flow and resulted in coolant over the blade. They also determined that film cooling effectiveness was higher near the trailing edge of the tip because of coolant accumulation.

Acharya et al. [2002] performed a computational study of squealer tip heat transfer that benchmarked experimental work by Azad et al. [2000]. Acharya et al. carried out a study beyond the benchmark to include injection cooling. They showed results that verified increased cooling effectiveness with increased blowing, but one result in particular stands out. Film coolant injection lowered the local pressure ratio altering the nature of the leakage vortex. Figure 2-18 shows the effect of film cooling on flow velocity through and around the tip gap. Without film cooling, high velocity flow leaks across the tip and then rolls into the leakage vortex on the suction side, which is shown as a region of lower velocity next to the mainstream flow. When film cooling is introduced, the coolant leaks across the tip in stripes of lower velocity air compared to the mainstream leakage. It was stated by Bindon [1989] that the leakage vortex is a result of the flow velocity difference between the accelerating tip leakage and the slower mainstream flow. The film cooling may serve to slow the tip leakage, reduce the relative velocity between the leakage and the mainstream flow, and, consequently, weaken the tip leakage vortex. The open literature points to injection cooling as a means of protecting a turbine tip from harmful leakage flow. There may be an added aerodynamic benefit of a weaker tip leakage vortex.

2.4 Uniqueness of Research

The objective of this research was to quantify the heat transfer effects of a microcircuit geometry placed in the tip that included injection from film holes along the pressure side of the blade. This geometry was developed by the sponsor, namely Pratt & Whitney. The tip clearance and blowing ratios were varied, and their effects were indicated with pressure coefficient contours on the shroud and with adiabatic effectiveness and cooling effectiveness contours on the tip surface. The research reported in this paper is set apart from that in open literature to date by more than the microcircuit geometry itself. This study is carried out on a large blade model with a large temperature difference between the mainstream and secondary flows so that effectiveness contours on the tip are reported with good resolution. Furthermore, this study reports effectiveness

contours based on temperatures that are recorded with an infrared camera rather than the more commonly used liquid crystal methods.

By measuring temperatures on a conductive tip material, as well as adiabatic surface temperatures, this study also takes a step towards a more complete heat transfer analysis that includes internal cooling effects of the microcircuit on the blade tip.

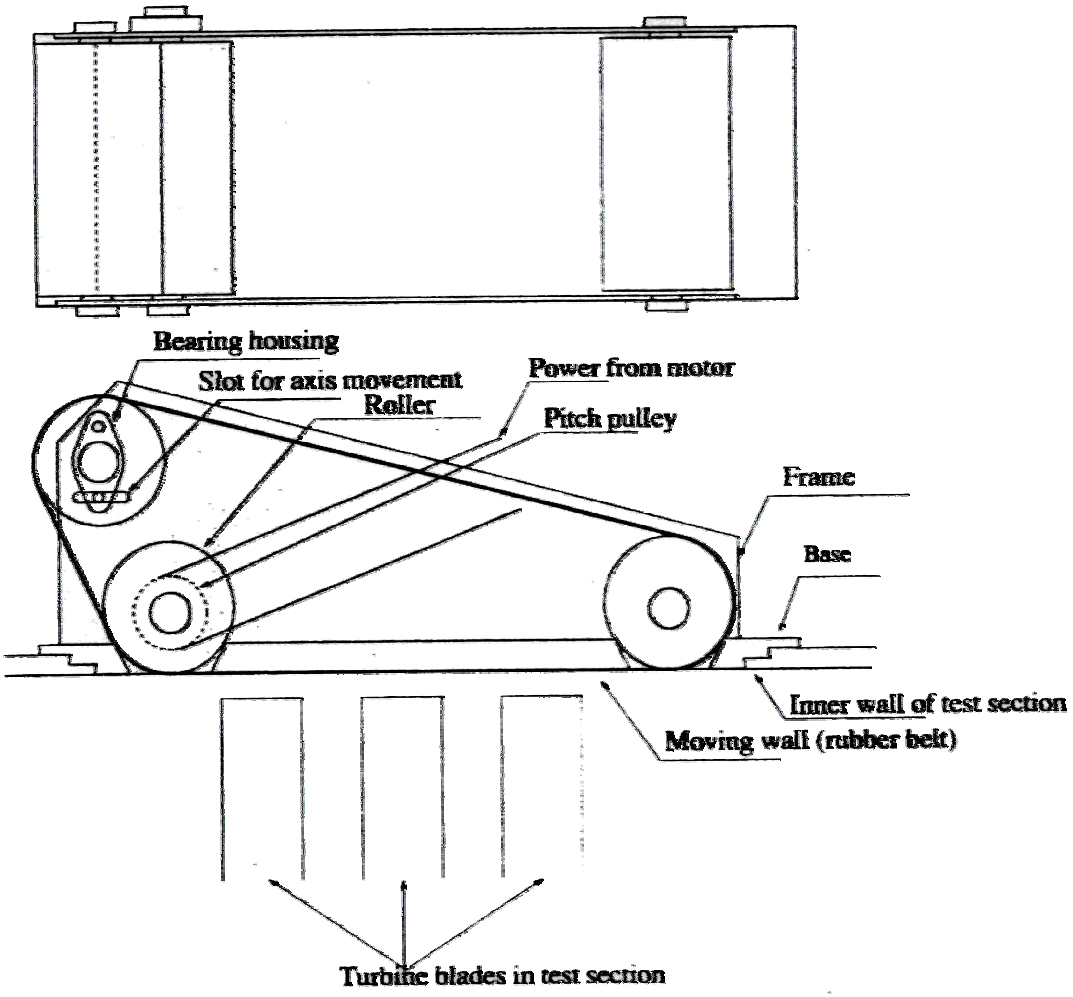

Figure 2-1 Diagram of moving wall apparatus used to simulate relative motion between the shroud and tip (Srinivasan and Goldstein, 2003).

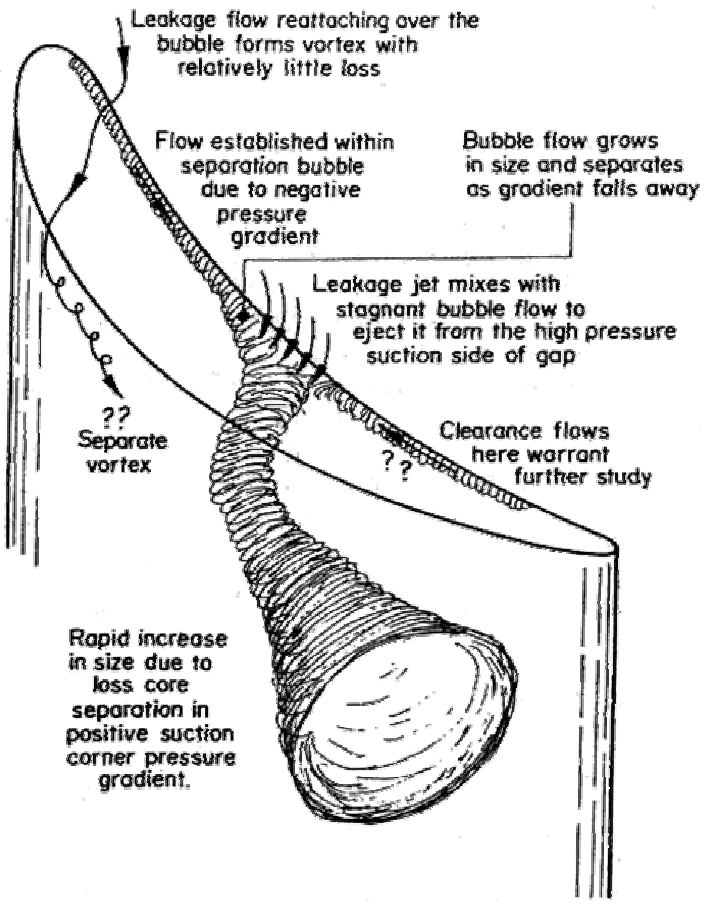

Figure 2-2 Separation bubble along the pressure side develops into tip leakage vortex off the suction side trailing edge (Bindon, 1989).

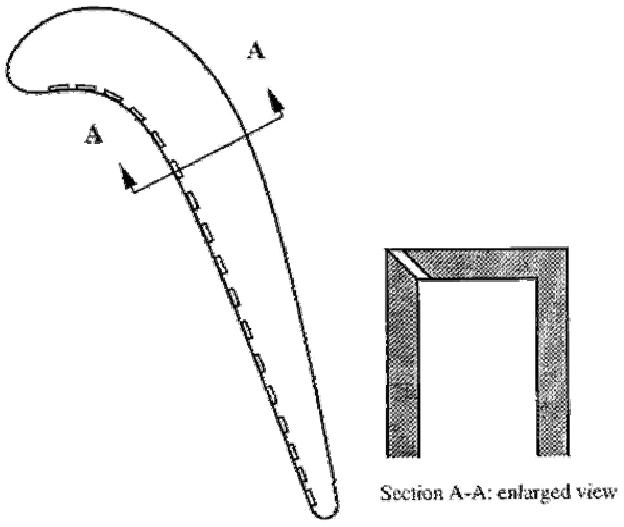

Figure 2-3 Tip blowing on the pressure side. The injection slots exit the blade tip at a 45° angle (Prasad, 1999).

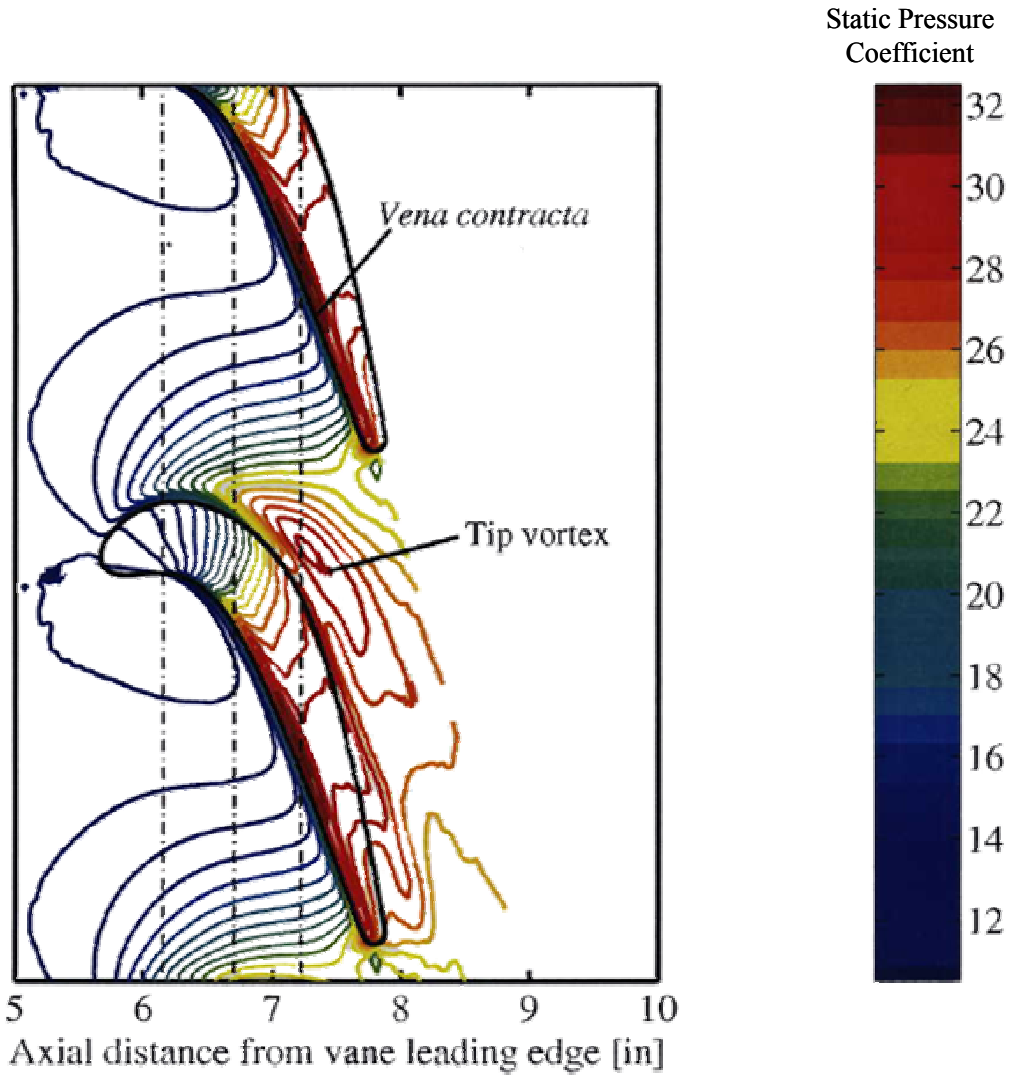

Figure 2-4 Pressure coefficient contours on the shroud for a flat tip without blowing. The tip vortex is located off the suction side near the blade's leading edge, while the *vena contracta* is on the pressure side of the tip near the trailing edge (Prasad, 1999).

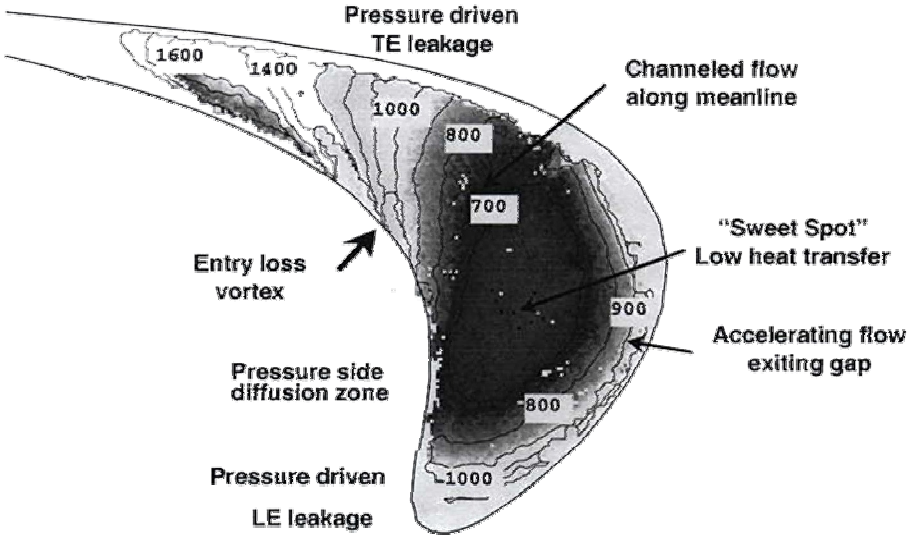

Figure 2-5 Heat transfer coefficient distribution in W / m^2 K for a flat blade with tip clearance at 1% of the total blade height (Bunker et al., 2000).

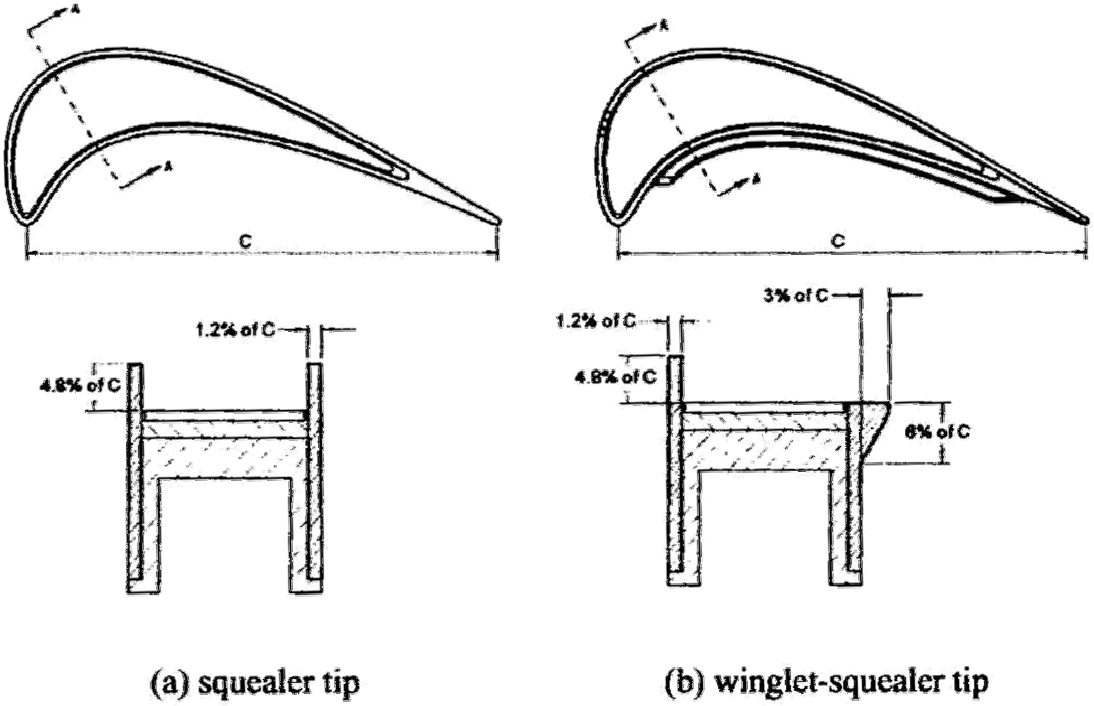

Figure 2-6 Layout of a a) squealer tip and b) winglet tip (Papa et al., 2003).

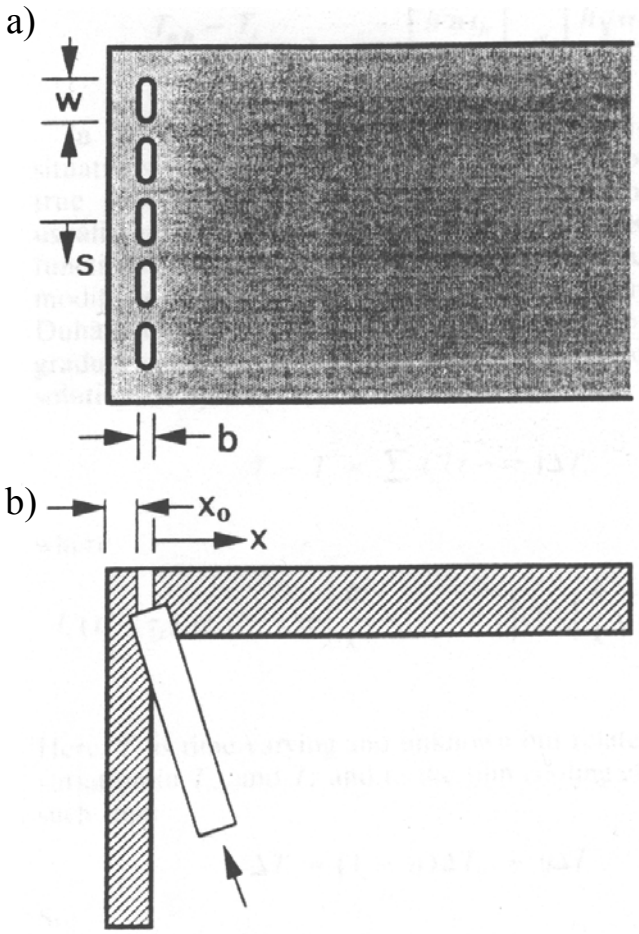

Figure 2-7 Film cooling hole pattern shown from a) the top and b) a side cross-sectional view (Kim and Metzger, 1995).

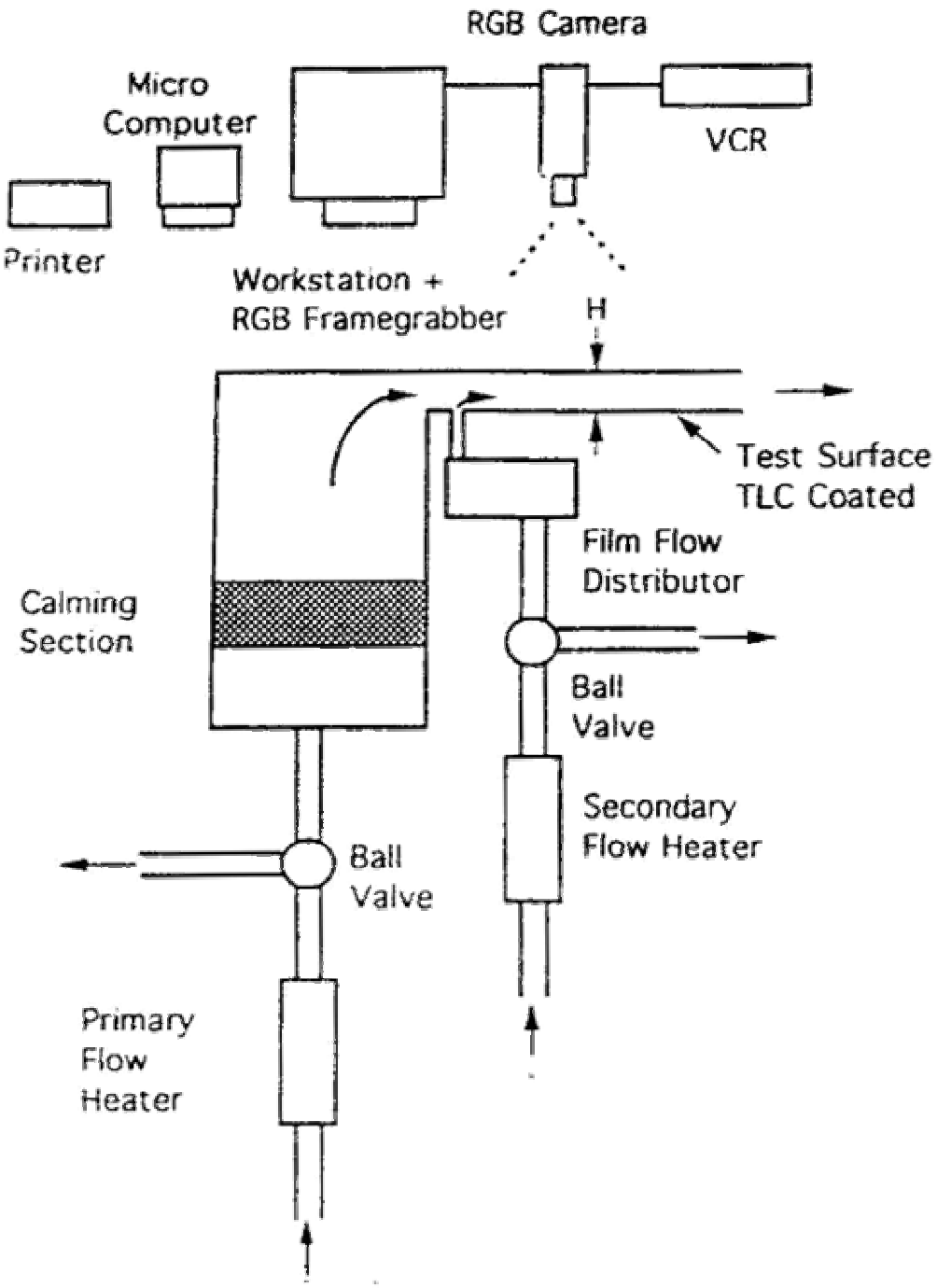

Figure 2-8 Experimental setup with computer visualization on the tip surface (Kim and Metzger, 1995).

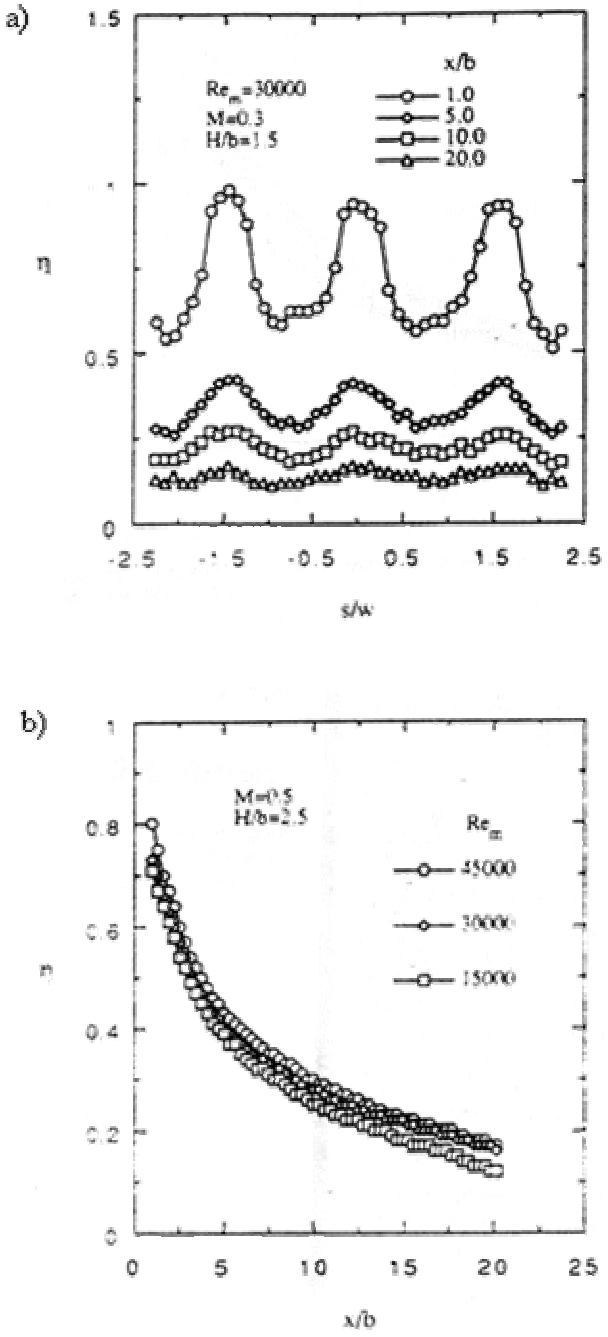

Figure 2-9 Film cooling effectiveness measurements a) made at four positions downstream of film cooling slots for a blowing ratio of M = 0.3 and Re = 30 x 10^3, and b) averaged across the span with a blowing ratio of M = 0.5 at three different Reynolds numbers (Kim and Metzger, 1995).